metals

MDPI

Article

The Mechanism of Inhomogeneous Grain Refinement in a NiTiFe Shape Memory Alloy Subjected to Single-Pass Equal-Channel Angular Extrusion

Yanqiu Zhang and Shuyong Jiang *

College of Mechanical and Electrical Engineering, Harbin Engineering University, Harbin 150001, China; zhangyq@hrbeu.edu.cn

* Correspondence: jiangshuyong@hrbeu.edu.cn; Tel.: +86-0451-8251-9710

Received: 6 September 2017; Accepted: 26 September 2017; Published: 29 September 2017

Abstract: Based on electron backscattered diffraction analysis and transmission electron microscopy observation, the mechanism of inhomogeneous grain refinement in a NiTiFe shape memory alloy (SMA) subjected to single-pass equal-channel angular extrusion (ECAE) was investigated. The results show that refined grains are mainly nucleated near grain boundaries and a small fraction of them emerges in the grain interior. The size of refined grains increases as deformation temperature increases, which indicates that a higher deformation temperature is adverse to grain refinement in the ECAE of NiTiFe SMAs. It is the accumulation and rearrangement of geometrically necessary dislocations as plastic strain increases that leads to the transition of lower angle subgrain boundaries, and finally higher angle subgrain boundaries are induced and finer grains are formed. Due to the limitation of slip systems, the mechanism of grain refinement in a NiTiFe SMA subjected to ECAE is different from that in face-centered cubic and body-centered cubic crystals. Dislocation cells and shear bands are two transition microstructures of grain refinement in the ECAE of NiTiFe SMAs. The nucleation of fine grains mainly occurs along shear bands or grain boundaries, which leads to the inhomogeneity of grain refinement.

Keywords: shape memory alloy (SMA); NiTiFe alloy; grain refinement; equal-channel angular extrusion (ECAE); microstructure

1. Introduction

As a functional material, NiTi-based shape memory alloys (SMAs) have been extensively applied in medical and engineering fields because they possess excellent superelasticity and perfect shape memory. It has been accepted that the functional performances of SMAs are closely related to their microstructures, where grain refinement is one of key factors. As a consequence, researchers have investigated the grain refinement of NiTi-based SMAs via various severe plastic deformation (SPD) methods, including cold rolling, high pressure torsion (HPT), surface mechanical attrition treatment (SMAT), local canning compression, cold drawing, and equal-channel angular extrusion (ECAE) [1–6]. Because the process of ECAE is relatively simple and can be used for manufacturing ultrafine-grained metals with relatively large sizes compared with other SPD methods, it is a potential technique for processing commercial ultrafine-grained metals. As a consequence, ECAE has increasingly gained attention over the last two decades [7–11]. So far, researchers have investigated the deformation behavior of ECAE in many conventional metals, such as magnesium alloys [12], steel [13], aluminum alloys [14], pure titanium [15], and pure copper [16]. These investigations mostly focused on the microstructures or mechanical properties of materials that have experienced multi-pass ECAE; the mechanism for grain refinement has not been thoroughly revealed.

It is widely accepted that the plastic deformation of metals results from dislocation slip or twinning, and different crystals possess different slip characteristics. The above conventional metals belong to face-centered cubic (FCC), body-centered cubic (BCC), or hexagonal close-packed (HCP) crystals. However, NiTi-based SMAs possess a B2 structure at the austenite state or a B19′ structure at martensite state. As a consequence, there should exist some differences between the NiTi-based SMAs and the above conventional metals. Even though several investigations on the ECAE of NiTi-based SMAs have been conducted, all of them have focused on the microstructures of ECAE at room temperature and the subsequent heat treatment, the effects of second phases on the mechanical properties and phase transformation, the influence of ECAE on shape memory response, or the damage tolerance of ECAE [17–23]. Up to now, no studies on the mechanism of grain refinement in ECAE of NiTi-based SMAs have been reported.

Therefore, the single-pass ECAE of an NiTiFe SMA at three different temperatures was performed in the present study so as to investigate the mechanism of inhomogeneous grain refinement in NiTiFe SMAs, where electron backscattered diffraction (EBSD) analysis and transmission electron microscopy (TEM) observation were conducted to produce the relevant data.

2. Materials and Methods

A commercially available NiTiFe SMA bar provided by Xi'an Saite Metal Materials Development Co., Ltd. (Xi'an, China) was used as the raw material in the current investigation [24]. The composition of the bar was $Ti_{50}Ni_{47}Fe_3$ (atom %), and the diameter of it was 9 mm. Three billets with a cross section of 5 mm × 5 mm and the length of 25 mm were taken from the as-received NiTiFe bar along the axis direction via a DK7725 type electro-discharge machine (EDM) (Jiangsu Dongqing CNC Machine Tool Co. Ltd., Taizhou, China). Subsequently, the NiTiFe billets experienced a single-pass ECAE via a die (Harbin Engineering University, Harbin, China) shown in Figure 1a at 400 °C, 450 °C, and 500 °C, respectively. The ECAE die possesses the channel cross section of 5 mm × 5 mm, and the radii of the upper and lower corners at the intersection between the inlet and outlet channels were set to 1 mm and 2 mm, respectively. The channel angle ϕ of the ECAE die was set to 120°, and the arc angle of the lower corner was set to 24°. The ECAE experiments were carried out via an INSTRON-5500R universal material testing machine (Instron Corporation, Norwood, MA, USA), where the velocity of the punch was set to 1.5 mm/min. Figure 1b illustrates the process of ECAE in the current investigation. In the present study, the equivalent strain ε induced by the single-pass ECAE can be obtained based on the equation proposed by Iwahashi et al. [25]:

$$\varepsilon = \frac{2\cot\left(\frac{\phi}{2}+\frac{\psi}{2}\right)+\psi\,\mathrm{cos\,ec}\left(\frac{\phi}{2}+\frac{\psi}{2}\right)}{\sqrt{3}}, \quad (1)$$

where ϕ is channel angle and ψ is the arc angle of the lower corner, as shown in Figure 1b. As a consequence, the equivalent strain in the present study was calculated as 0.63.

After the extrusion, slice specimens with a size of 5 mm × 5 mm were taken from the as-received sample and the three ECAE samples, respectively, where the sampling planes are parallel to the longitudinal sections of the samples, as shown in Figure 1b,c. Subsequently, they were processed for EBSD analysis and TEM observation. Before the EBSD analysis, the slice specimens experienced mechanical polishing and subsequent electro-polishing so that strain-free surfaces were acquired. The EBSD analysis was conducted via a field-emission scanning electron microscope (SUPRA 55 SAPPHIRE, University of South Carolina, Columbia, SC, USA) equipped with an EBSD detector. During EBSD analysis, the relationship between the crystal coordinate and the sample coordinate of the as-received sample was set to (100)//TD, (010)//RD, and (001)//ND, where TD, RD, and ND represent the transverse direction, the rolling direction, and the normal direction of the as-received sample, respectively. However, the relationship between the crystal coordinate and the sample coordinate of the ECAE samples was set to (100)//ED, (010)//TD, and (001)//ND, where ED, TD,

and ND represent the extrusion direction, the transverse direction, and the normal direction of the ECAE sample, respectively. The sample systems for the as-received and ECAE samples are shown in Figure 1b,c, respectively. Before TEM observation, the foils were firstly ground to 70 μm by the mechanical method and then thinned by the twin-jet method in the electrolyte, with a composition of 34% $CH_3(CH_2)_3OH$, 6% $HClO_4$, and 60% CH_3OH (in volume). Afterward, TEM observation was performed via an FEI TECNAI G2 F30 microscope (Field Electron and Ion Company, Hillsboro, OR, USA).

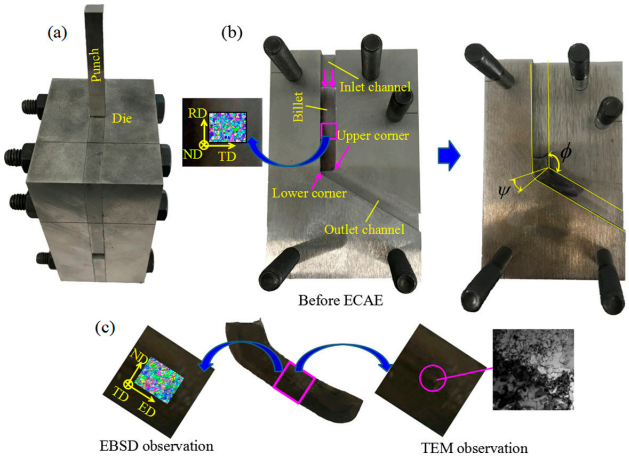

Figure 1. Experimental illustration of equal-channel angular extrusion (ECAE): (**a**) ECAE die; (**b**) process of ECAE; (**c**) sampling location for analysis (In the case of as-received sample, TD, RD, and ND represent the transverse direction, the rolling direction, and the normal direction. In the case of ECAE sample, ED, TD, and ND represent the extrusion direction, the transverse direction, and the normal direction, respectively. TEM: Transmission electron microscopy; EBSD: Electron backscattered diffraction).

3. Results

Figure 2 illustrates the EBSD results of the as-received NiTiFe SMA by means of orientation imaging microscopy (OIM; Technische Universität Bergakademie Freiberg, Freiberg, Germany), where a boundary misorientation criterion of 15° was used in the present study. As seen in Figure 2a, all the grains present an approximately equiaxed shape. In addition, it can be found from Figure 2b that the majority of the grains possess an equivalent grain diameter ranging from 3 μm to 15 μm, and the size of the largest grain is lower than 30 μm.

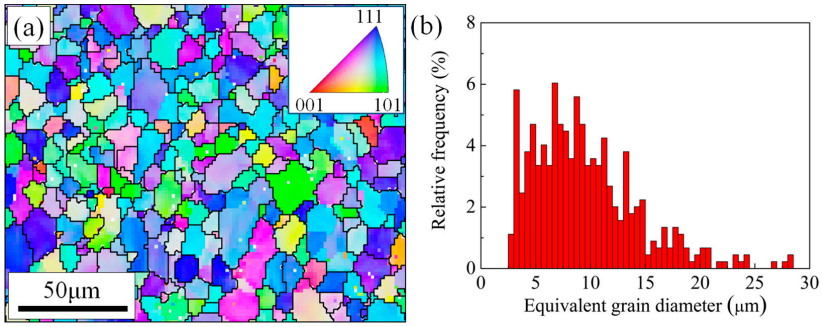

Figure 2. Electron backscattered diffraction (EBSD) results of the as-received NiTiFe shape memory alloy (SMA) by means of orientation imaging microscopy (OIM): (**a**) Microstructure; (**b**) histogram of equivalent grain diameter.

Figure 3 illustrates the OIM microstructures of the NiTiFe SMA subjected to ECAE at various temperatures. It can be seen that the microstructures of the NiTiFe SMA present inhomogeneity after the single-pass ECAE, where a number of elongated or equiaxed fine grains arise in the grain interior and at the grain boundaries of the remained coarse grains. Meanwhile, the remained coarse grains of all three NiTiFe samples are elongated slightly along the shear direction of ECAE, which is inclined by about 60° with respect to the loading direction. It can be also seen that the numbers of the fine grains in the samples subjected to ECAE at 400 °C and 450 °C are much greater than the one in the sample subjected to ECAE at 500 °C. The phenomenon indicates that the deformation temperature has a significant effect on the microstructure of NiTiFe SMA subjected to single-pass ECAE. In order to investigate the effect of deformation temperature on the grain size of the sample subjected to ECAE, histograms of equivalent grain diameter for the three samples are illustrated in Figure 4. It can be found that the number of grains lower than 5 μm decreases as deformation temperature increases, which indicates that lower ECAE temperature is beneficial to the refinement of grains. In addition, it can be observed that the sizes of the largest grains in the three ECAE samples are all larger than the one in the as-received sample. The aforementioned phenomenon indicates that the single-pass ECAE performed at temperatures ranging from 400 °C to 500 °C is not only able to lead to the refinement of some grains, but can also coarsen the remained coarse grains. The driving force for the growth of remained coarse grains properly comes from deformation-stored energy in them, and the mechanism for this phenomenon is unclear and will be investigated in a future study.

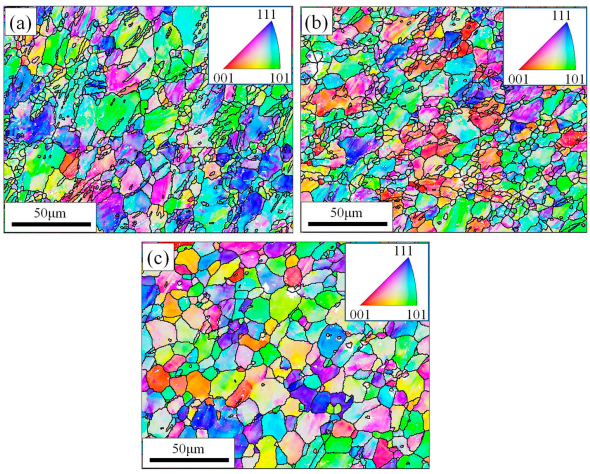

Figure 3. OIM microstructures of the NiTiFe SMA subjected to ECAE at various temperatures: (**a**) 400 °C; (**b**) 450 °C; (**c**) 500 °C.

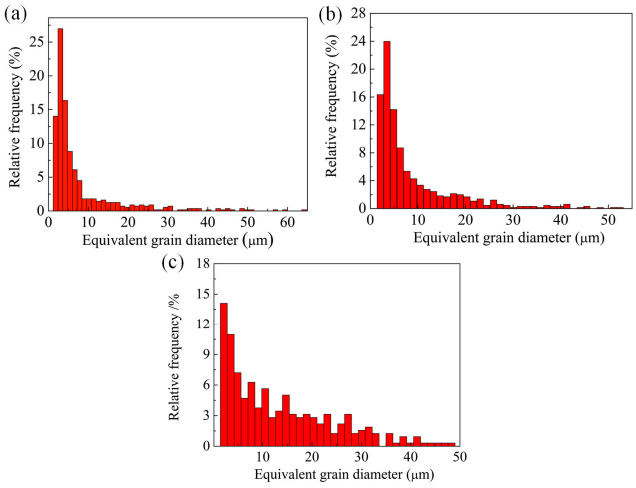

Figure 4. Histograms of equivalent grain diameter for the NiTiFe SMA subjected to ECAE at various temperatures: (**a**) 400 °C; (**b**) 450 °C; (**c**) 500 °C.

In order to reveal the substructure evolution in the grains of NiTiFe SMA subjected to ECAE, distributions of kernel average misorientation (KAM) in the three samples are calculated, as shown in Figure 5. It can be seen that the subgrain boundaries induced in the NiTiFe samples subjected to ECAE at 400 °C and 450 °C are much greater than the ones in the NiTiFe sample subjected to ECAE at 500 °C. In addition, there are many subgrain boundaries with higher misorientation angles in the grain interior and near the grain boundaries of the former two samples. The above phenomena indicate that the grain refinement of ECAE results from the transition of lower angle grain boundaries to higher ones, and lower deformation temperature is able to induce more substructures during the ECAE of NiTiFe SMA. As a consequence, the NiTiFe SMA is not suitable for being processed by ECAE at temperatures above 500 °C due to its weak ability of grain refinement.

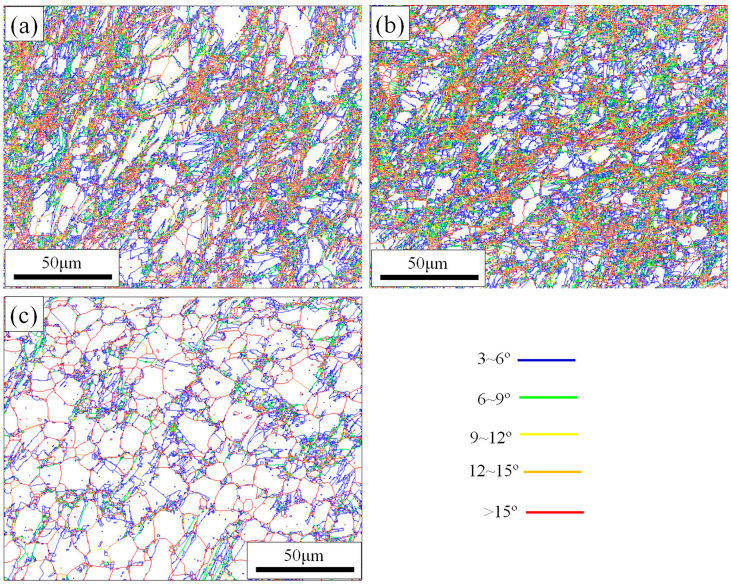

Figure 5. Distributions of kernel average misorientation (KAM) in the NiTiFe SMA subjected to ECAE at various temperatures: (**a**) 400 °C; (**b**) 450 °C; (**c**) 500 °C.

It has been accepted that there is deformation inhomogeneity both among the grains and in the grain interior. Consequently, geometrically necessary dislocations (GNDs) will be induced to accommodate the deformation inhomogeneity so that the material is not fractured. For the purpose

of investigating the influence of temperature on the deformation in homogeneity in the NiTiFe SMA subjected to ECAE, geometrically necessary dislocation (GND) distributions in the three samples are calculated based on EBSD data, as shown in Figure 6. According to the concept of GND, the region with a higher density of GNDs indicates a higher inhomogeneity of deformation. It can be seen in Figure 6 that, in the samples subjected to ECAE at 400 °C and 450 °C, the area with a higher density of GNDs is much larger than that in the sample subjected to 500 °C. Furthermore, the regions with a higher density of GNDs are in accordance with those with higher misorientations, as shown in Figure 5. This phenomenon occurs because subgrain boundaries disturb the coordination between the two parts beside the boundary, and more GNDs are required to adjust the deformation coordination. It is the accumulation and rearrangement of these GNDs as plastic strain increases that leads to the transition of lower angle subgrain boundaries. Finally, higher angle subgrain boundaries are induced, and finer grains are formed.

For the purpose of investigating the mechanism of grain refinement at a more microscopic scale, TEM micrographs of the three samples are obtained, as shown in Figure 7. It can be seen that in the case of ECAE at 400 °C, several dislocation cells and some shear bands can be observed in a zone of about 3×3 μm^2, and some subgrains and fine grains can be found in a region of about 1.6×1.6 μm^2. In the case of ECAE at 450 °C, only two fragmentary dislocation cells and one fine grain can be observed in a region of about 4×4 μm^2. However, as for the ECAE at 500 °C, only a fragmentary dislocation cell can be seen in a region of about 3×3 μm^2, and no subgrains or fine grains are observed. The aforementioned phenomena indicate that the size of dislocation cells increases as ECAE temperature increases, and the number of subgrains decreases as ECAE temperature increases. The evidence demonstrates that the fine grains of the NiTiFe SMA subjected to single-pass ECAE might be related to the dislocation cells, and a lower deformation temperature leads to a higher density of dislocation cells. Furthermore, the grain refinement during the ECAE of a NiTiFe SMA might also result from the shear bands.

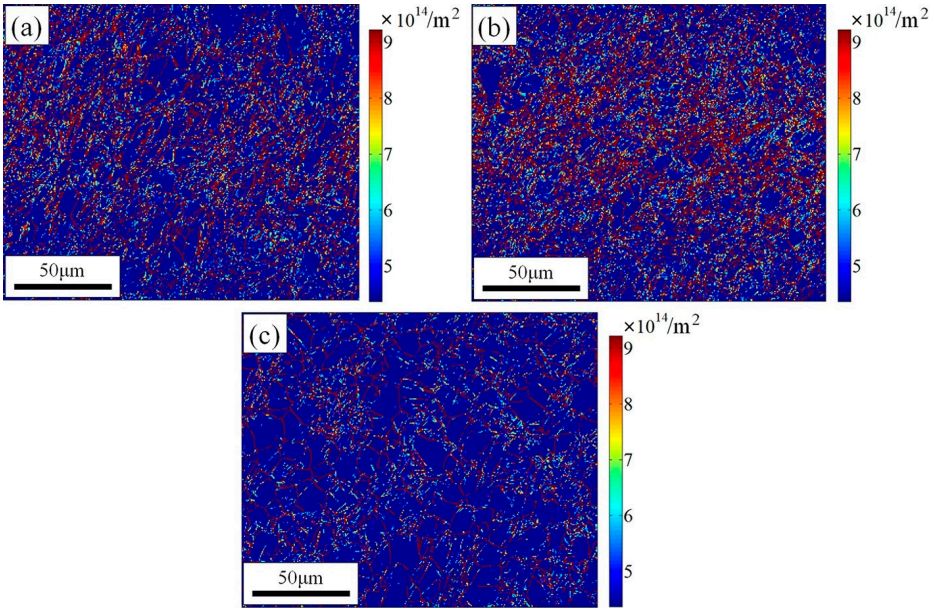

Figure 6. Geometrically necessary dislocation (GND) distributions in the NiTiFe SMA subjected to ECAE at various temperatures: (**a**) 400 °C; (**b**) 450 °C; (**c**) 500 °C.

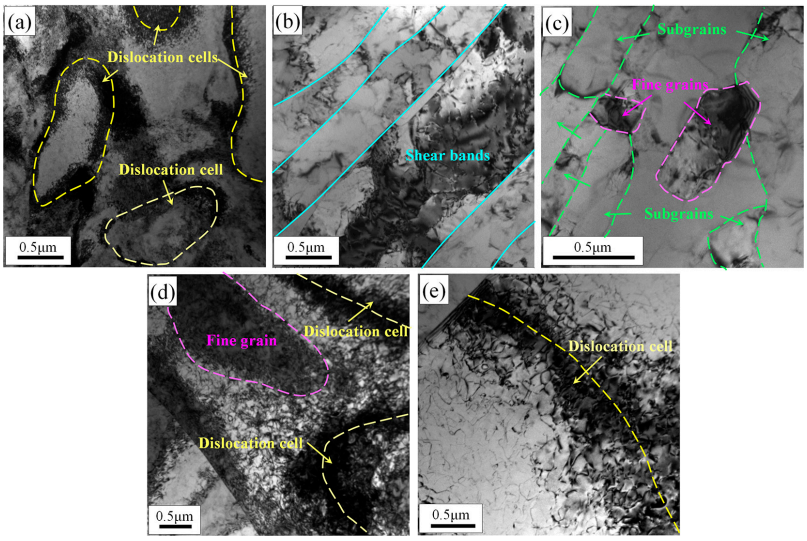

Figure 7. Transmission electron microscopy (TEM) micrographs of the NiTiFe SMA subjected to ECAE at various temperatures: (**a**) Dislocation cells at 400 °C; (**b**) shear bands at 400 °C; subgrains and fine grains at (**c**) 400 °C; (**d**) 450 °C; (**e**) 500 °C.

4. Discussion

Based on the aforementioned results, it can be concluded that single-pass ECAE performed at 400–500 °C is able to refine the grains of NiTiFe SMA. However, the obtained microstructures present a high inhomogeneity, where the refined grains are mainly nucleated near the grain boundaries and a small fraction of them emerges in the grain interior. In addition, the grain size of NiTiFe SMA subjected to ECAE increases as deformation temperature increases. Based on these evidences and the information on substructure distributions, GND density distributions, and TEM micrographs, the mechanism of grain refinement in the NiTiFe SMA subjected to ECAE can be proposed, as shown in Figure 8.

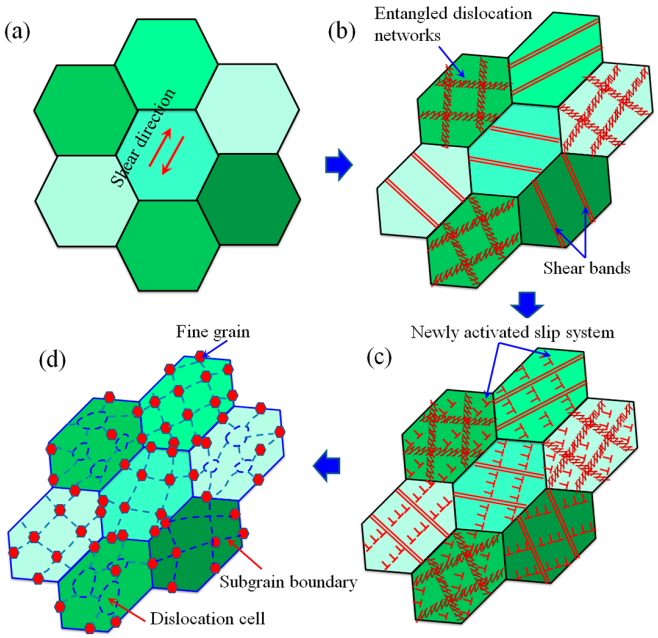

Figure 8. The proposed mechanism for the grain refinement of NiTiFe SMA subjected to single-pass ECAE: (**a**) Equiaxed coarse grains before ECAE; (**b**) microstructure at the early stage of ECAE, showing original coarse grains being elongated along the shear plane and the formation of shear bands and entangled dislocation networks; (**c**) the activation of other slip systems and the block of later induced dislocations; (**d**) rearrangement of dislocations, formation of dislocation cells, subgrains and newly fine grains induced by continuous recovery (In the figure, different background colors represent different orientations).

It is well known that the structure of NiTiFe SMA is B2 austenite above room temperature. It has been accepted that the B2 cubic austenite of NiTi-based SMA is composed of two simple cubic lattices, where each simple cubic lattice consists of eight Ni atoms or eight Ti atoms. According to previous studies, the slip systems found in B2 austenite of NiTi-based SMA are the <100>{001}, <100>{011}, and <111>{110} families, where the <100>{011} family is the most likely to be activated one because it requires the least stacking fault energy and the least critical stress for plastic deformation [26–28]. As a consequence, the <100>{011} family will be activated at an early stage of ECAE. According to the crystallographic characteristics of cubic crystals, there are six {011} planes in B2 austenite of NiTi-based SMAs, and only one direction is allowed to slip in each {011} plane. Therefore, there are only six possible slip systems in the <100>{011} family of the NiTiFe SMA. This number is only a half of those in FCC and BCC crystals, which both possess 12 slip systems. Therefore, the mechanism of ECAE in NiTiFe SMAs is different from that in FCC and BCC crystals. In the two crystals, the SPD leads to the simultaneous activation of two or more slip systems in a grain, which induces numerous complicated networks that are composed of dislocation entanglements. With increasing strain, GNDs are accumulated in these dislocation networks, which increase misorientations among them. As a result, subgrains and subsequent grain refinement can be achieved when the misorientations reach a certain critical value. It has been proved that the <100>{011} family only permits the occurrence of slip in three independent slip systems, including [100](011), [010](101), and [001](110) [28,29]. In addition, according to Schmid's law, the initially activated slip systems are those possessing the largest value of the Schmid factor because minimum force is required [24].The value of the Schmid factor is related to the loading direction and the orientation of an individual grain. In addition, because there are angles among the three independent slip systems, their Schmid factors are unable to reach the maximum value at the same time. As a consequence, in a B2 austenite grain, only one or two of the three systems may be activated at the same time due to the limitation of slip system number. In the case of one activated

slip system alone, shear bands are dominant at the early stage of ECAE. In the case of two activated slip systems, entangled dislocation networks are dominant at the initial stage of ECAE. Figure 8a illustrates the equiaxed coarse grains before ECAE, and Figure 8b shows the microstructure at the early stage of ECAE, where original coarse grains are elongated along the shear plane by shear deformation, and shear bands and entangled dislocation networks are induced in the grain interior. It has been widely accepted that both slip and orientation rotation are induced during plastic deformation. As a result, with the proceeding of ECAE, other slip systems will be activated when the orientation rotation causes the inactivated systems of the <100>{011} family to turn to a preferred orientation or when the stress is high enough for activating the slip systems of the <100>{001} and <111>{110} families. At this stage, the slip of dislocations induced later will be blocked by the shear bands, the grain boundaries, and the dislocation networks. Dislocation pile-ups are formed when they are blocked by shear bands or grain boundaries, while the blocked dislocations are absorbed by the dislocation networks when they meet the dislocation networks. Figure 8c illustrates the activation of other slip systems and the block of dislocations induced later. Shortly after the deformation, continuous recovery occurs, which leads to the rearrangement of dislocations, the formation of dislocation cells, subgrains, and newly fine grains, as shown in Figure 8d. The nucleation of the fine grains mainly occurs along the shear bands or the grain boundaries. This is due to the fact that a high density of dislocations is blocked by the shear bands as well as the grain boundaries. These dislocations are continuously trapped at low angle boundaries in these regions when they attempt to pass through them, which leads to the increase in GNDs and the subsequent formation of newly fine grains. The above mechanism illustrates why the grain refinement in NiTiFe SMAs subjected to single-pass ECAE is inhomogeneous.

Although ECAE is able to refine the grains of metals, the deformation temperature should be considered when the parameters are determined. Higher temperature may lower the dislocation densities during ECAE or will lead to fast growth of the refined grains, which both fail to refine the grains. Lower temperatures can produce higher dislocation densities and maintain the overall fine grains, but it faces the risk of material fracture. In the current investigation, the temperature over 500 °C is not suitable for the ECAE processing of NiTiFe SMAs, which can be confirmed by the weak grain refinement shown in Figure 3c.

5. Conclusions

(1) Single-pass ECAE performed at 400–500 °C is able to refine the grains of a NiTiFe SMA. However, the obtained microstructures present a high inhomogeneity, where the refined grains are mainly nucleated near the grain boundaries and a small fraction of them emerges in the grain interior. Furthermore, the size of the refined grains increases as ECAE temperature increases, which indicates that the higher deformation temperature is adverse to the refinement of ECAE.

(2) The grain refinement of ECAE results from the transition of lower angle grain boundaries to higher ones, and a lower deformation temperature is able to induce more substructures during the ECAE of a NiTiFe SMA. The ECAE of NiTiFe SMAs is not suitable for being performed at temperatures above 500 °C due to its weak ability of grain refinement. It is the accumulation and rearrangement of GNDs as plastic strain increases that leads to the transition of lower angle subgrain boundaries. Higher angle subgrain boundaries are finally induced, and finer grains are formed.

(3) Due to the limitation of slip systems, the mechanism of grain refinement in NiTiFe SMA subjected to single-pass ECAE is different from that in FCC and BCC crystals. Dislocation cells and shear bands are two transition microstructures of grain refinement during the ECAE of NiTiFe SMAs. The nucleation of the fine grains mainly occurs along the shear bands or the grain boundaries, which leads to the inhomogeneity of grain refinement.

Acknowledgments: The work was financially supported by the National Natural Science Foundation of China (No. 51475101 and No. 51305091).

Author Contributions: Yanqiu Zhang performed EBSD (electron backscattered diffraction) and TEM (transmission electron microscopy) analysis and wrote the manuscript; Shuyong Jiang supervised the research.

Conflicts of Interest: The authors declare no conflict of interest.

References

1. Tsuchiya, K.; Inuzuka, M.; Tomus, D.; Hosokawa, A.; Nakayama, H.; Morii, K.; Todaka, Y.; Umemoto, M. Martensitic transformation in nanostructured TiNi shape memory alloy formed via severe plastic deformation. *Mater. Sci. Eng. A* **2006**, *438–440*, 643–648. [CrossRef]
2. Khaleghi, F.; Khalil-Allafi, J.; Abbasi-Chianeh, V.; Noori, S. Effect of short-time annealing treatment on the superelastic behavior of cold drawn Ni-rich NiTi shape memory wires. *J. Alloys Compd.* **2013**, *554*, 32–38. [CrossRef]
3. Peterlechner, M.; Waitz, T.; Karnthaler, H.P. Nanoscale amorphization of severely deformed NiTi shape memory alloys. *Scr. Mater.* **2009**, *60*, 1137–1140. [CrossRef]
4. Zhang, Y.; Jiang, S.; Hu, L.; Liang, Y. Deformation mechanism of NiTi shape memory alloy subjected to severeplastic deformation at low temperature. *Mater. Sci. Eng. A* **2013**, *559*, 607–614. [CrossRef]
5. Jiang, S.; Zhao, Y.; Zhang, Y.; Tang, M.; Li, C. Equal channel angular extrusion of NiTi shape memory alloy tube. *Trans. Nonferr. Met. Soc. China* **2013**, *23*, 2021–2028. [CrossRef]
6. Hu, T.; Chen, L.; Wu, S.L.; Chu, C.L.; Wang, L.M.; Yeung, K.W.K.; Chu, P.K. Graded phase structure in the surface layer of NiTi alloy processed by surface severe plastic deformation. *Scr. Mater.* **2011**, *64*, 1011–1014. [CrossRef]
7. Li, S.; Beyerlein, I.J.; Necker, C.T. On the development of microstructure and texture heterogeneity in ECAE via route C. *Acta Mater.* **2006**, *54*, 1397–1408. [CrossRef]
8. Su, C.W.; Lu, L.; Lai, M.O. A model for the grain refinement mechanism in equal channel angular pressing of Mg alloy from microstructural studies. *Mater. Sci. Eng. A* **2006**, *434*, 227–236. [CrossRef]
9. Qarni, M.J.; Sivaswamy, G.; Rosochowski, A.; Boczkal, S. On the evolution of microstructure and texture in commercial purity titanium during multiple passes of incremental equal channel angular pressing (I-ECAP). *Mater. Sci. Eng. A* **2017**, *699*, 31–47. [CrossRef]
10. Frint, S.; Hockauf, M.; Frint, P.; Wagner, M.F.X. Scaling up Segal's principle of equal-channel angular pressing. *Mater. Des.* **2016**, *97*, 502–511. [CrossRef]
11. Li, H.; Li, S.; Zhang, D. On the selection of outlet channel length and billet length in equal channelangular extrusion. *Comput. Mater. Sci.* **2010**, *49*, 293–298. [CrossRef]
12. Cheng, W.; Tian, L.; Wang, H.; Bian, L.; Yu, H. Improved tensile properties of an equal channel angular pressed (ECAPed) Mg-8Sn-6Zn-2Al alloy by prior aging treatment. *Mater. Sci. Eng. A* **2017**, *687*, 148–154. [CrossRef]
13. Hao, T.; Tang, H.; Luo, G.; Wang, X.; Liu, C.; Fang, Q. Enhancement effect of inter-pass annealing during equal channel angular pressing on grain refinement and ductility of 9Cr1Mo steel. *Mater. Sci. Eng. A* **2016**, *667*, 454–458. [CrossRef]
14. Sitdikov, O.; Avtokratova, E.; Sakai, T. Microstructural and texture changes during equal channel angular pressing of an Al-Mg-Sc alloy. *J. Alloys Compd.* **2015**, *648*, 195–204. [CrossRef]
15. Qarni, M.J.; Sivaswamy, G.; Rosochowski, A.; Boczkal, S. Effect of incremental equal channel angular pressing (I-ECAP) on the microstructural characteristics and mechanical behaviour of commercially pure titanium. *Mater. Des.* **2017**, *122*, 385–402. [CrossRef]
16. Gholami, D.; Imantalab, O.; Naseri, M.; Vafaeian, S.; Fattah-alhosseini, A. Assessment of microstructural and electrochemical behavior of severely deformed pure copper through equal channel angular pressing. *J. Alloys Compd.* **2017**, *723*, 856–865. [CrossRef]
17. Shahmir, H.; Nili-Ahmadabadi, M.; Mansouri-Arani, M.; Langdon, T.G. The processing of NiTi shape memory alloys by equal-channel angularpressing at room temperature. *Mater. Sci. Eng. A* **2013**, *576*, 178–184. [CrossRef]
18. Shahmir, H.; Nili-Ahmadabadi, M.; Wang, C.T.; Jung, J.M.; Kim, H.S.; Langdon, T.G. Annealing behavior and shape memory effect in NiTi alloy processed by equal-channel angular pressing at room temperature. *Mater. Sci. Eng. A* **2015**, *629*, 16–22. [CrossRef]

19. Zhang, D.; Guo, B.; Tong, Y.; Tian, B.; Li, L.; Zheng, Y.; Gunderov, D.V.; Valiev, R.Z. Effect of annealing temperature on martensitic transformation of $Ti_{49.2}Ni_{50.8}$ alloy processed by equal channel angular pressing. *Trans. Nonferr. Met. Soc. China* **2016**, *26*, 448–455. [CrossRef]
20. Kockar, B.; Karaman, I.; Kulkarni, A.; Chumlyakov, Y.; Kireeva, I.V. Effect of severe ausforming via equal channel angular extrusion on the shape memory response of a NiTi alloy. *J. Nucl. Mater.* **2007**, *361*, 298–305. [CrossRef]
21. Song, J.; Wang, L.; Zhang, X.; Sun, X.; Jiang, H.; Fan, Z.; Xie, C.; Wu, M.H. Effects of second phases on mechanical properties and martensitic transformations of ECAPed TiNi and Ti-Mo based shape memory alloys. *Trans. Nonferr. Met. Soc. China* **2012**, *22*, 1839–1848. [CrossRef]
22. Leitner, T.; Sabirov, I.; Pippan, R.; Hohenwarter, A. The effect of severe grain refinement on the damage tolerance of a superelastic NiTi shape memory alloy. *J. Mech. Behav. Biomed. Mater.* **2017**, *71*, 337–348. [CrossRef] [PubMed]
23. Kocich, R.; Szurman, I.; Kursa, M.; Fiala, J. Investigation of influence of preparation and heat treatment on deformation behaviour of the alloy NiTi after ECAE. *Mater. Sci. Eng. A* **2009**, *512*, 100–104. [CrossRef]
24. Zhang, Y.; Jiang, S.; Wang, S.; Sun, D.; Hu, L. Influence of partial staticrecrystallization on microstructures and mechanical properties of NiTiFe shape memory alloysubjected to severe plastic deformation. *Mater. Res. Bull.* **2017**, *88*, 226–233. [CrossRef]
25. Iwahashi, Y.; Wang, J.; Horita, Z.; Nemoto, M. Principle of equal-channel angular pressing for the processing of ultra-fine grained materials. *Scr. Mater.* **1996**, *35*, 143–146. [CrossRef]
26. Gall, K.; Dunn, M.L.; Liu, Y.; Labossiere, P.; Sehitoglu, H.; Chumlyakov, Y.I. Micro and macro deformation of single crystal NiTi. *J. Eng. Mater. Technol.* **2002**, *124*, 238–245. [CrossRef]
27. Benafan, O.; Noebe, R.D.; Padula, S.A.; Garg, A.; Clausen, B.; Vogel, S.; Vaidyanathan, R. Temperature dependent deformation of the B2 austenite phase of a NiTi shape memory alloy. *Int. J. Plast.* **2013**, *51*, 103–121. [CrossRef]
28. Ezaz, T.; Wang, J.; Sehitoglu, H.; Maier, H.J. Plastic deformation of NiTi shape memory alloys. *Acta Mater.* **2013**, *61*, 67–78. [CrossRef]
29. Pelton, A.R.; Huang, G.H.; Moinec, P.; Sinclair, R. Effects of thermal cycling on microstructure and properties in Nitinol. *Mater. Sci. Eng. A* **2012**, *532*, 130–138. [CrossRef]